Report no. 00/08

The Influence of Unstructured Mesh Type on the Prediction of Convoluted Shear Layers

Hayder Salman, James J. McGuirk, Gary J. Page,
Department of Aeronautical and Automotive Engineering
Loughborough University

Pierre Moinier
Oxford University
Numerical Analysis Group

Lobed mixers are used in gas turbine engines to enhance mixing between hot and cold streams and to reduce noise. Computational modelling of such systems has previously been carried out on structured meshes, although mesh generation difficulties have encouraged the use of unstructured tetrahedral meshes. However, the ability of numerical schemes to predict the mixing behaviour correctly on tetrahedral meshes has not been studied and is the subject of this work. Three different mesh types for the mixing region resolution have been studied: purely hexahedral, purely tetrahedral, and a mixed mesh combining hexahedra, tetrahedra and pyramids. Results are presented for the evolution of both a planar and a convoluted turbulent shear layer. In regions of high shear, misalignment of control volume faces has a major influence on spurious numerical spreading of the shear layer. For the tetrahedral mesh, there is an initial rapid mixing, followed by a reduction in mixing rate. The smoothing terms present are triggered by the combination of a high gradient across a control volume face and a velocity normal to that face; this occurs on the diagonal edges of tetrahedral meshes. The magnitude of the spurious smoothing is diminished by increasing the aspect ratio of the cells. For lobed mixer predictions, a mixed mesh with aligned high aspect ratio hexahedral elements in the shear layer region and pyramids and tetrahedra linking to the outer domain provides a good compromise between ease of mesh generation and quality of solution.

Oxford University Computing Laboratory
Numerical Analysis Group
Wolfson Building
Parks Road
Oxford, England OX1 3QD

May, 2000

Contents

1 INTRODUCTION

Lobed mixers are passive mixing devices providing augmentation of the mixing between two coflowing streams. These devices, which have demonstrated much benefit in terms of improved mixing with minimum pressure losses, have become a common component of a modern gas turbine engine. The lobed mixer consists of a splitter plate separating the two streams with a corrugated trailing edge. The corrugations create radial deflections of each stream through the lobes but in opposite directions. At the mixer's trailing edge, the two streams interact. Velocity differences present between the two streams cause a convoluted shear layer to form with a waveform equivalent to the mixer's trailing edge. Superimposed on this shear layer are regions of streamwise vorticity of alternating sign arising due to the radially deflected flows as observed by Paterson [7]. Within a small distance from the trailing edge, the streamwise vorticity causes the convoluted shear layer structure to rotate encompassing a large portion of the flow domain as seen in Fig. 1. These convoluted shear layers, together with the complex

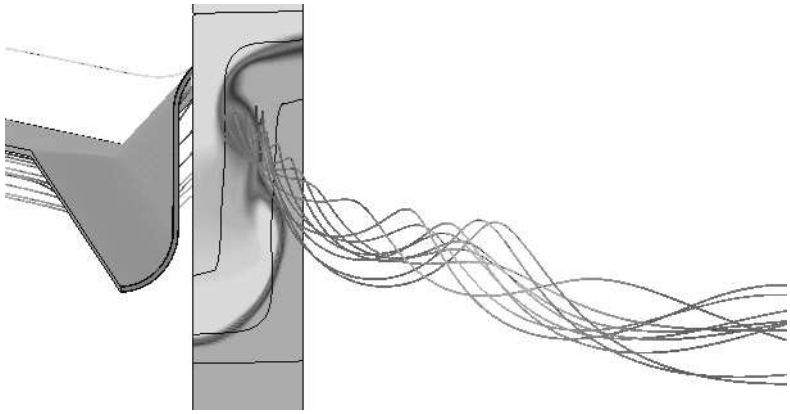

Figure 1: Interaction of the streamwise vortex with the convoluted shear layer

nature of mixer configurations encountered, has resulted in the classification of lobed mixer flows as complex flows. To model them successfully, meshes have to be generated which correctly represent the mixer whilst at the same time being appropriate for the capture of the mixing layers.

The computational modelling of such flows has been carried out predominantly through the use of structured grids. A recent study, employing a multi-block structured grid with body-fitted curvilinear coordinates, was performed by Salman et al. [5] to model the mixer configuration used here. This reference contains a review of computational modelling of mixers prior to 1999. All studies to date with such grids have highlighted grid generation as one of the key difficulties in modelling these flows. It is thus believed that ultimately unstructured grids will be necessary to capture the geometric complexity of the mixer. The use of unstructured grids for lobed mixers has been rare. Konrad et al. [3] used tetrahedral meshes to model the flow over a scarfed mixer. A more fundamental study using tetrahedral grids was conducted by O'Sullivan et al. [12]. However, neither study was able to demonstrate, how accurately the convoluted shear layers were being modelled. In particular, the effects of the tetrahedral grids used on the solution quality compared to the more widely used hexahedral grids is an area that has so far escaped attention.

For Euler problems unstructured grids have demonstrated much potential, particularly when used with adaptive techniques. Having tackled the nonlinear convective terms, one

might expect extension to the Navier Stokes equations to be straightforward. However, the presence of thin, viscously dominated boundary layers around a body can only be resolved efficiently through the use of highly stretched anisotropic elements. This reintroduces a form of structure into the grid normal to the surface in these regions. Such an approach is often seen in 2D aerofoil calculations. An O-Grid of highly stretched elements is wrapped around the body with isotropic triangular elements used in the rest of the flow domain. The use of such an approach raises two issues. Firstly, generating such grids is not necessarily a straightforward task, particularly for 3D cases. Secondly, not every form of high stretching is effective. In 2D, for example, the accuracy of a Finite Element approximation on triangular elements degrades as the maximum angle of the element increases. In a Finite Volume formulation, the accuracy will depend on how control volumes are constructed (e.g. median dual or containment dual). Indeed, since some form of structured clustering of the elements is required, the current trend is towards hybrid grids. Quadrilateral elements in 2D, and prismatic or hexahedral elements in 3D are used next to a solid surface.

In principle the concepts described above work well when the viscous effects are confined to thin regions near solid bodies and the direction in which gradients are high is known in advance. In lobed mixer flows the viscous effects quickly spread throughout the flow domain. In addition, due to the formation of a convoluted shear layer, the direction of the normal gradients in the shear layer is not known *a priori*. These features combine to raise difficulties in the modelling of these shear layers and begin to seriously test modern unstructured solvers in predicting viscous flows.

The objective of the present work is to illustrate and investigate three different meshing strategies for lobed mixers with varying levels of automation of the grid generation process. This will include a purely hexahedral grid, a mixed tetrahedral/prismatic grid, and a mixed hexahedral/tetrahedral/pyramidal grid. An important aspect of this study is to quantify the accuracy of the predictions for these different mesh types through detailed comparisons of local and global parameters. This forms a necessary step in assessing the suitability of unstructured methods for modelling complex mixer configurations.

The paper will begin with a description of the numerical scheme employed in this study. A description of the mixer configuration and the flow conditions simulated is presented in section (3). Illustrations of the grids used are presented in section (4). Results are then presented, firstly for a 2D planar shear layer. This will be used to study the sensitivity of the numerical solutions of shear flows to different grids in a simplified setting. The additional issues of resolving the geometrical and flow complexity of the lobed mixer convoluted shear layer are then presented.

2 NUMERICAL SCHEME DESCRIPTION

The equations that are solved are the steady, compressible, Reynolds-averaged Navier-Stokes equations, which appear in semi-discrete form as

$$\frac{dQ}{dt} + R(Q) = 0 \tag{2.1}$$

where Q denotes the set of conservative variables, and $R(Q)$ is the residual vector of the spatial discretisation.

Using a finite volume approach, the discrete approximation of the residual for an interior grid point is

$$R_j = \frac{1}{V_j} \sum_{i \in E_j} F_{ij} \triangle s_{ij} \quad \forall j \tag{2.2}$$

where V_j is the size of the control volume (the median-dual) associated with index j, E_j the set of all nodes connected to node j via an edge, $\triangle s_{ij}$ a face length (2D) or area (3D) associated with the edge, and F_{ij} is the numerical flux.

At a solid wall, an extra term from the boundary faces associated with the node is added. Tangency and no-slip wall conditions are enforced by zeroing out the momentum components associated with the corresponding wall condition, whereas the far field boundary is treated by adding an extra upwinded flux difference.

The inviscid flux discretisation is based on the flux-differencing ideas of Roe [10], combining central differencing of the non-linear inviscid fluxes with a smoothing term based on one-dimensional characteristic variables. This numerical dissipation is a blend of second and fourth characteristic differences with a limiter Ψ. Thus, the inviscid numerical flux takes the following form

$$\begin{aligned} F_{ij}^I &= \frac{1}{2} \left(\mathcal{F}_{ij}^I(Q_i) + \mathcal{F}_{ij}^I(Q_j) \right. \\ &- \left. |A_{ij}| \left(-\frac{1}{3}(1-\Psi)(\hat{L}_i^{lp}(Q) - \hat{L}_j^{lp}(Q)) + \Psi(Q_i - Q_j) \right) \right) \end{aligned} \tag{2.3}$$

where $\hat{L}^{lp}$ is a linear transparent pseudo Laplacian [6]. The viscous flux is approximated halfway along each edge and uses the usual integration rule around each control volume, giving a consistent finite volume treatment of the inviscid and viscous terms. The equations are time integrated using the 5-stage Runga-Kutta method of Martinelli [4].

At low Mach number the disparity between the acoustic and convective wave speeds cannot be adequately handled by the current approach, and a slowdown of the convergence is observed. Furthermore, the numerical solution produced is often of poor quality with significant errors in the pressure distribution due to the relative scaling of the different numerical smoothing terms. To address these difficulties, the inviscid equations are preconditioned by an invertible matrix Γ expressed in symmetrised variables. The resulting numerical flux thus becomes

$$\begin{aligned} F_{ij}^I &= \frac{1}{2} \left(\mathcal{F}_{ij}^I(Q_i) + \mathcal{F}_{ij}^I(Q_j) \right. \\ &- \left. P_{ij}\Gamma_{ij}^{-1} |\Gamma_{ij}\tilde{A}_{ij}| P_{ij}^{-1} \left(-\frac{1}{3}(1-\Psi)(\hat{L}_i^{lp}(Q) - \hat{L}_j^{lp}(Q)) + \Psi(Q_i - Q_j) \right) \right) \end{aligned} \tag{2.4}$$

where $P_{ij} = M_{ij}N_{ij}$ and M and N are the transformation matrices from primitive variables to conservative variables, and from symmetrised variables to primitive variables, respectively. Only the dissipation has changed, which makes the implementation attractive as it does not require any change of variables in the current code. Details concerning the low Mach number preconditioner and its formulation are given in [6].

To improve convergence rates and to overcome discrete stiffness in the equations, a matrix time step or preconditioner is also used. Its effect is to cluster the eigenvalues of the residual

spatial operator in a region of the complex plane where the iterative method has good damping properties. In this work the block Jacobi preconditioner is used, as in previous work with the turbulent Navier-Stokes equations on unstructured grids [6], and earlier on structured grids [9].

Thus, the pre-conditioned semi-discrete equation appears as

$$P^{-1}\frac{dQ}{dt} + R(Q) = 0 \tag{2.5}$$

where P^{-1} is the local point-implicit block-Jacobi preconditioner [11, 1]. The preconditioner P is based on a local linearisation of the 3D Navier-Stokes equations about a uniform flow, and built by extracting the terms corresponding to the central node. As the flux can be split into inviscid and viscous parts, the matrix preconditioner has contributions coming from both. Details of its construction are given in [6].

To account for the effects of turbulence, the two equation $k-\epsilon$ turbulence model of Launder and Spalding [2] with wall functions is used. An important requirement that must be fulfilled by the time integration procedure, is the positivity of the turbulence variables k and ϵ. To achieve this, a point-implicit treatment is adopted for the source terms. The equations are then integrated using the same Runga-Kutta method as used for the flow equations.

3 MIXER CONFIGURATION

The mixer configuration studied is the same as that modelled computationally in Salman et al. [5]. Details of the mixer configuration studied are given in Fig. 2. The important parameters are the lobe wavelength (λ), the lobe height (h), and the lobe inclination angle (φ). A schematic of the mixer configuration is also shown in the figure. The wind-tunnel cross section is 198mm wide by 200mm high.

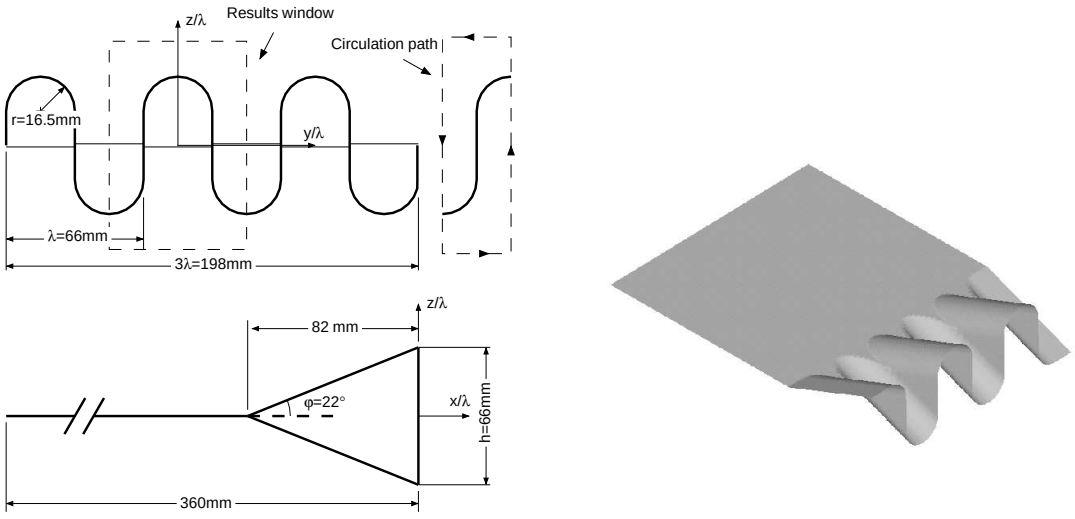

Figure 2: Definition of the mixer configuration investigated

To reduce the problem size and simplify the computations carried out here, a perfectly periodic flow structure is assumed within the mixing region. This simplification implies the

presence of planes of symmetry between adjacent streamwise vortices such that only half a lobe need be modelled. This assumption is not strictly valid as pointed out in Salman et al. [5], but is justifiable for the issues being addressed here.

Air at standard temperature and pressure was used as the working fluid in the current work. The studies were carried out with the two streams set at a static pressure ratio and density ratio of 1.0. The velocities were set to $6ms^{-1}$ (U_{low}) in the slow stream and $10ms^{-1}$ (U_{high}) in the fast stream corresponding to Mach numbers of 0.0176 and 0.0294 respectively. The inlet boundary conditions for the turbulence quantities in the $k-\epsilon$ equations were evaluated based on a turbulence intensity of 1% and an eddy viscosity equal to the molecular viscosity. At inlet constant profiles were assumed. The top and bottom tunnel walls were modelled as slip walls. The above conditions are identical to those used in the study of Salman et al. [5].

4 GRID GENERATION

Grids generated for the half lobe section described above are shown in Figs. 3, 4, and 5. To allow appropriate comparisons to be made between the various grids, the number of unknowns should be similar. In a cell vertex scheme, the unknowns are stored at nodal locations of the primal grid. Thus, all three grids were generated with approximately 150,000 nodes.

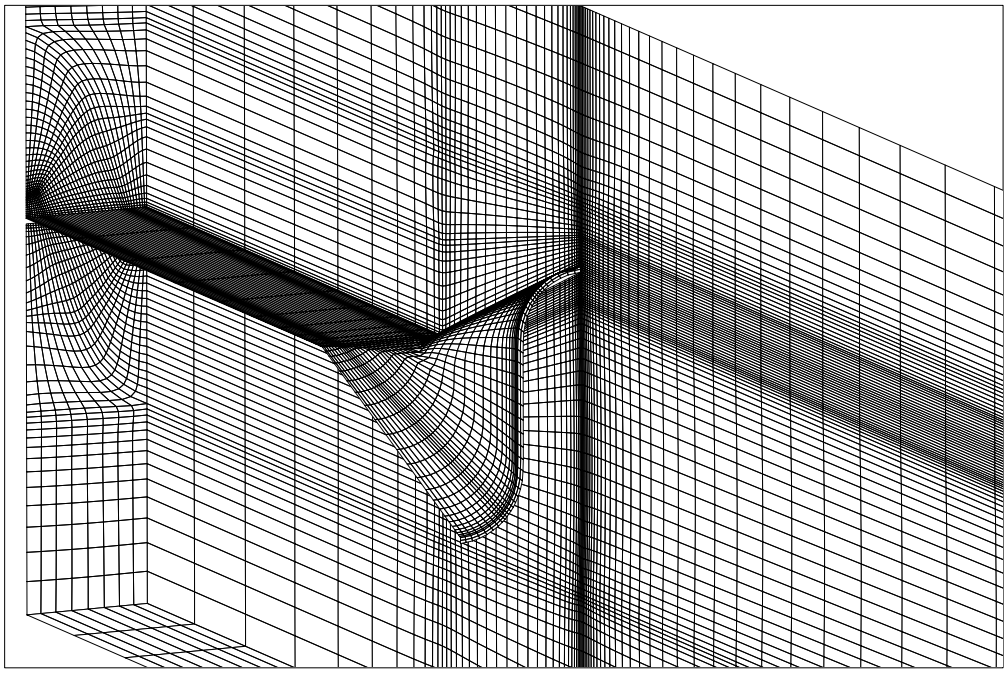

Figure 3: Unstructured hexahedral grid

The hexahedral grid is shown in Fig. 3. This grid consists of a similar topology to the multi-block structured grid studied in Salman et al. [5]. The benefits of this topology are the improved grid orthogonality within the mixing region and the ability to capture the mixer surface with a body-fitted grid. Further upstream, the grid orthogonality is sacrificed but the flow there is predominantly inviscid. Hexahedral elements allow highly stretched elements to be used without deterioration of solution quality. This feature was employed in the streamwise

direction where high grid resolutions are not required as axial gradients were generally smaller. An obvious problem is the inefficient clustering of grids (e.g. wasted elements in the upstream region where the flow is essentially uniform).

A second meshing strategy employing a fully automated process for generating the lobed mixer grid is shown in Fig. 4. The grid consists of two element types, prism elements, and tetrahedral elements. This approach allows the mixer geometry to be easily captured and has the potential of being easily extended to more complex mixers. A structured layer of prism elements is generated normal to the mixer surface to resolve the boundary layer efficiently. Tetrahedral elements are then used to fill the remainder of the computational domain. Unlike the hexahedral grids, this approach provides significant computational savings upstream of the mixer where the flow is uniform and much coarser grids can be used. However, efficient resolution of the boundary layer requires highly stretched elements in the streamwise direction. Since prism elements are generated from triangular elements on a surface, anisotropic triangular elements are therefore required. Additionally a layer of highly stretched tetrahedra joining the prisms would need to be generated. Generating such highly stretched elements with the software used presented problems. This limitation resulted in less efficient resolution of the

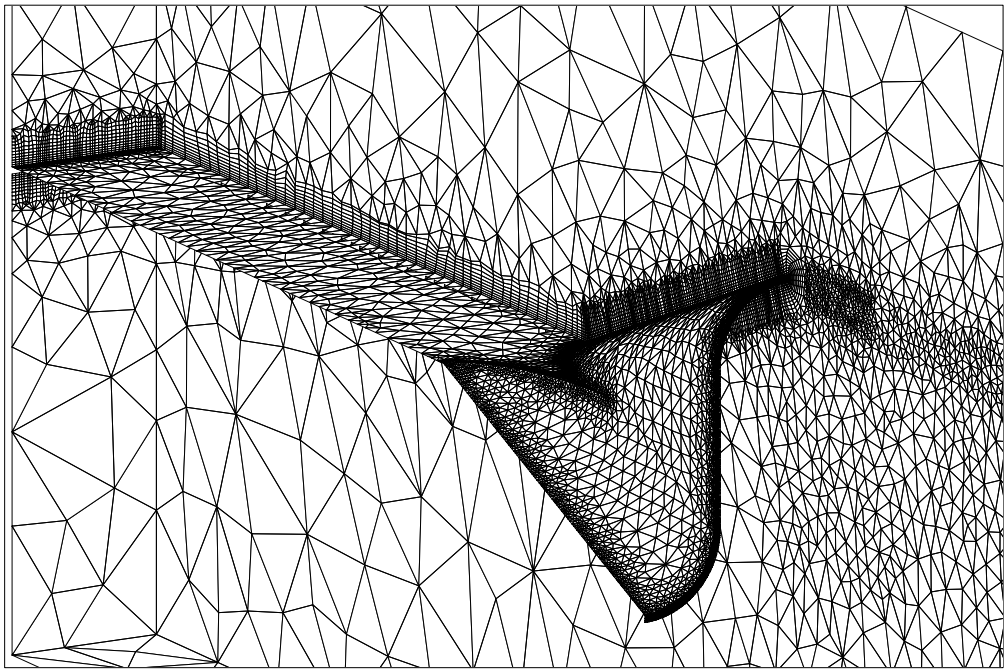

Figure 4: Unstructured tetrahedral grid

boundary layers with this grid. In the present study, this grid will simply be referred to as the tetrahedral grid since only tetrahedral elements were used within the mixing region where the focus of interest lies for the current work.

Finally, a mesh that employed hexahedral, tetrahedral, and pyramidal elements was studied as shown in Fig. 5. This strategy provides an intermediate approach, semi-automating the grid generation, but allowing control of the hexahedral parts of the grid. In principal, such an approach should combine advantages from both of the first two strategies. Tetrahedral grids are used in inviscid parts of the flow where flow gradients are much smaller and alignment of the grid with the flow is not required. In the viscous regions, hexahedral grids are used to

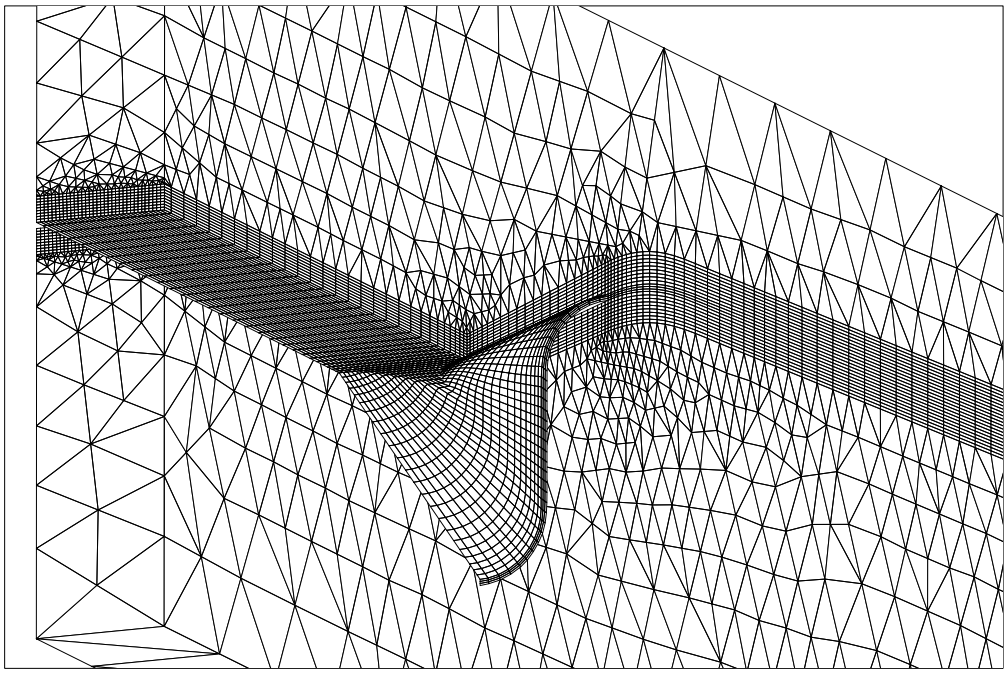

Figure 5: Unstructured mixed grid

resolve the boundary and shear layers. The ability to generate stretched hexahedral elements that do not deteriorate solution quality should allow these flow features to be resolved more efficiently than with the tetrahedral grid. The two mesh types are then joined together at the interface through transition pyramidal elements. In practice, one finds difficulties in using highly stretched hexahedral grids. Such grids cause pyramidal elements with highly skewed surfaces to be generated. Problems consequently arise in generating tetrahedral grids at the interface with the pyramidal elements. To remedy this difficulty, the grid resolution in the streamwise direction is increased to reduce the aspect ratios of the quadrilateral faces which form the bases of the pyramidal elements. This modification allowed the grid to be successfully completed with the grid generation software used. As pointed out earlier, a high grid resolution is required only in a direction normal to the shear layer. Thus, this increased resolution in the streamwise direction provides a degrading of efficiency in the mixed grid. For brevity, in the text that follows, this grid will simply be referred to as the mixed grid.

5 RESULTS

5.1 Planar shear layer

As a preliminary test, calculations will be presented for a 2D planar shear layer. Studies concerned with the planar shear layer, both computationally and experimentally, are extensively documented in the literature (e.g. Wilcox [13]). This provides a benchmark study for which the mixing behaviour is well known. Moreover, it contains similar viscous/ turbulent mixing processes to those that occur in the convoluted shear layers of lobed mixers. Studying the sensitivity of the predicted shear layers in this simplified flow helps understand some of the underlying numerical issues in modelling mixing type problems on quadrilateral and triangular

grids. The planar shear layer removes the problem of efficiently clustering the grid cells as the mixing layer position is known in advance.

The planar shear layer was computed with the same inlet conditions as those used in the lobed mixer studies. Computations were performed on three grid types as shown in Fig. 6. These included a purely quadrilateral mesh, three triangular meshes, and a mixed mesh. Three of these grids contained the same nodal distribution within the shear layer region. The nodal

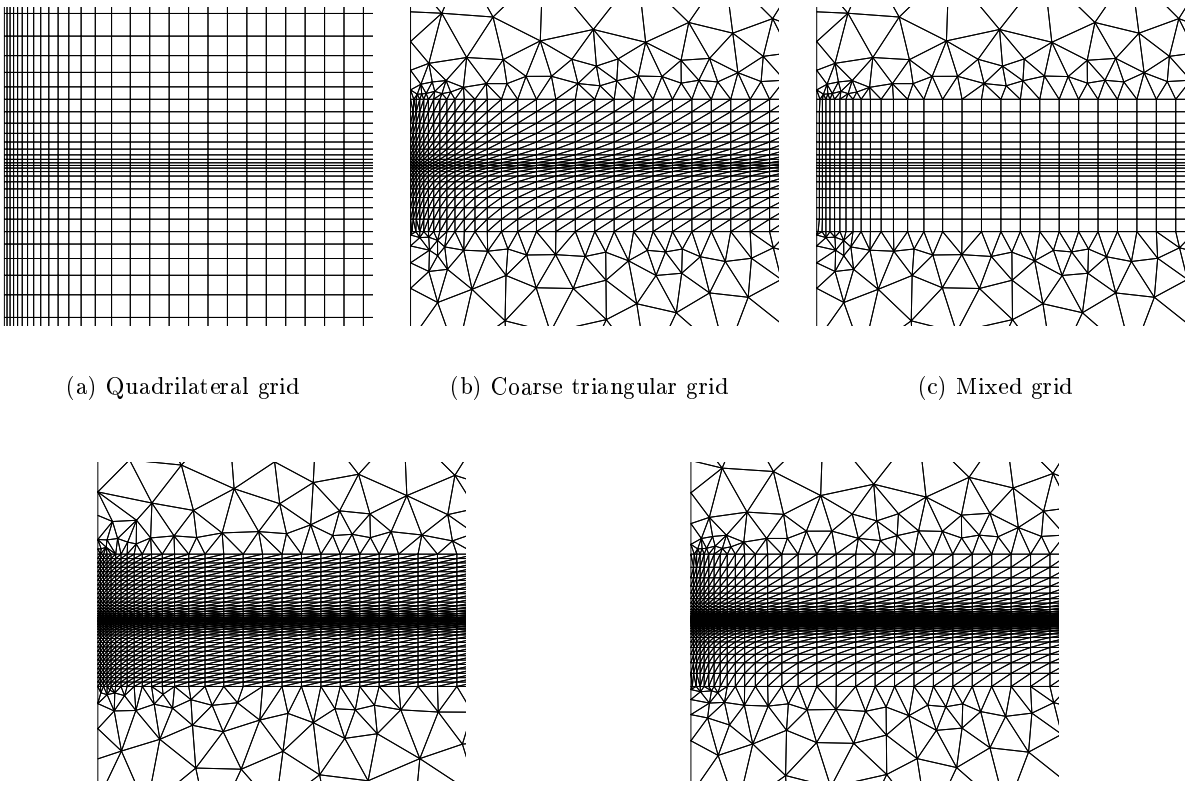

(a) Quadrilateral grid (b) Coarse triangular grid (c) Mixed grid

(d) Refined triangular grid (1st case) (e) Refined triangular grid (2nd case)

Figure 6: Planar shear layer grids near the inlet

distribution was modified for the last two grids shown in Fig. 6 for reasons described below. Thus the same three meshing strategies presented in section (4) for the lobed mixers have been studied here.

An important property of the planar shear layer is the concept of self-similarity which the flow attains at sufficiently large Reynolds numbers and downstream distance. Under these conditions the mean and turbulent quantities at different streamwise locations assume profiles, which when scaled with the local shear layer thickness, have the same shape. This so called self-preserving behaviour is associated with a linear growth of the planar mixing layer. The behaviour can be correctly predicted only if the correct physical mixing is simulated. The spreading rate parameter can therefore be used as a quantitative measure of the level of mixing being predicted. The mixing layer thickness, d_{layer}, is defined as the distance between the points in the mean velocity profile where the square of the non-dimensional mean velocity is

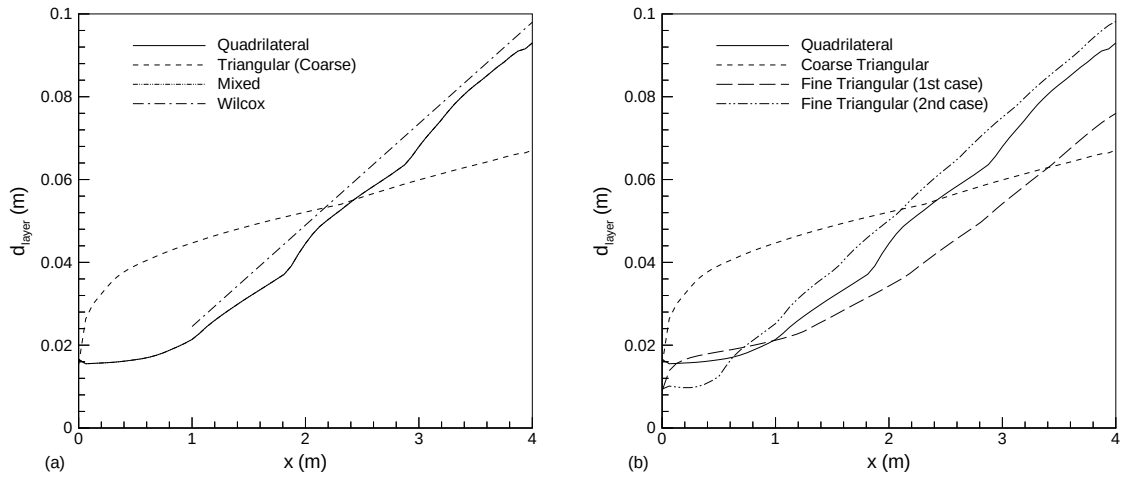

(a) Comparison of different grid types

(b) Comparison of triangular grids

Figure 7: Variation of shear layer thickness with downstream distance

0.1 and 0.9 respectively. The non-dimensional mean velocity is given by

$$U^* = \frac{U - U_{low}}{U_{high} - U_{low}} \tag{5.1}$$

Figure 7(a) presents the spreading of the mixing layer with downstream distance for grids (a), (b), and (c). A reference result for the self-similar spreading rate taken from Wilcox [13] has also been included using the same $k - \epsilon$ model.

Results for the quadrilateral grid reveal the correct spreading has been obtained with just eight nodes found across the mixing layer by $x = 4m$. The coarse triangular mesh shows a very different behaviour. This is seen via a very rapid growth of the shear layer within the first $1m$. The spreading then decreases rapidly such that it is approximately 40% of the correct spreading rate by $x = 2m$.

To identify the reasons for these results, two aspects of the discretisation are considered. Firstly, differences in control volumes between the triangular and quadrilateral grids associated with cells lying within the shear layer are shown in Fig. 8. Additionally, one needs to recall from section (2) that the inviscid fluxes include a smoothing term based on one-dimensional characteristic variables. This one dimensional decomposition is performed in a direction normal to the control volume faces. In a shear layer flow, the transverse components of velocity are much smaller than the streamwise components. Therefore, the flow is more or less aligned with horizontal control volume faces and perpendicular to vertical faces. The resulting numerical smoothing is thus very small in the quadrilateral grid. When moving to control volumes as in triangular grids, as shown in Fig. 8, control volume faces exist whose normal is oblique to the main flow direction. When performing the 1D decomposition into characteristic variables on such faces, a significant contribution will arise in the cross stream direction resulting in higher numerical smoothing than in the quadrilateral grid. This accounts for the higher spreading occurring in the early stages of the shear layer indicated in the results. The increased spreading reduces gradients across the layer resulting in lower production of turbulent energy and hence

eddy viscosity. The rapid decrease in spreading rate that follows is believed to be a direct consequence of this drop in turbulent energy. The arguments presented above suggest that reducing the angle (γ) defined in Fig. 8, such that the oblique control volume faces become more aligned with the flow, may reduce numerical smoothing. This can be achieved either by increasing the grid spacing (Δx) in the streamwise direction or reducing the cell height (Δy).

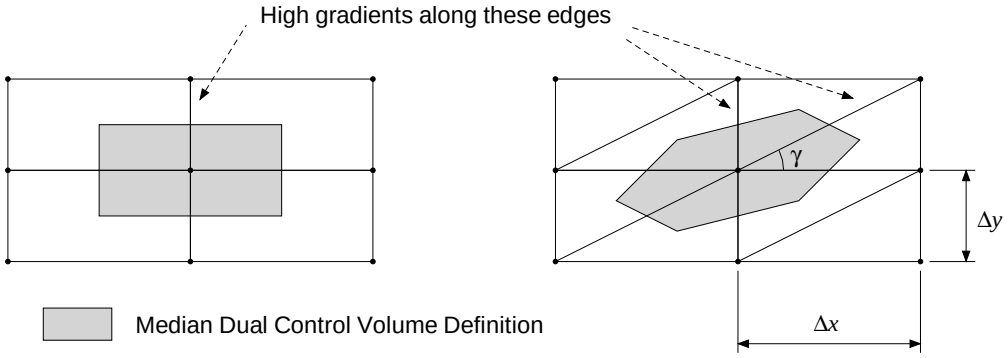

Figure 8: Form of control volumes within the shear layer region obtained by using quadrilateral and triangular grids

The calculations for the triangular grid were repeated with two more cases. Firstly, the grid resolution across the shear layer was doubled. Results for this case are shown in Fig. 7(b) together with the quadrilateral and coarse triangular grid solutions. This case is labeled as the fine triangular (1st case). Results now show a much lower spreading in the early stages compared to the coarse triangular grid solution. Further downstream, the flow is able to recover reaching the expected self-similar behaviour. The problems encountered in the early stages are associated with the low aspect ratio ($\Delta x/\Delta y$) elements present in this region. A second refined grid was therefore studied. This consisted of an equal number of nodes as the first refined grid. However, the nodes were redistributed across the shear layer to reduce the aspect ratios of the elements at the inlet. The shear layer spreading for this case also shown in Fig. 7(b) clearly demonstrates the reduced numerical smoothing which then results.

Unstructured triangular grids clearly have an advantage in providing more efficient clustering of the grid. However, this simple study has demonstrated the superiority of quadrilateral elements in terms of solution accuracy. These findings motivate a mixed grid approach to tackling the shear layer problem. An example of a prediction using a mixed quadrilateral/triangular grid is included in Fig. 7(a) corresponding to the mesh presented in Fig. 6(c). The grid consisted of 1531 nodes compared to the 2880 nodes found in the quadrilateral grid. The spreading rate coincides with the solution from the quadrilateral grid. The solution quality illustrates clearly the potential for such an approach to produce high quality numerical solutions at reduced computational cost.

5.2 Convoluted shear layer

In the convoluted shear layers, additional complexities arise in producing appropriate 3D unstructured meshes as discussed in section (4). In particular the issues raised in the previous section for triangular grids can be very serious for tetrahedral grids. Generating high aspect ratio tetrahedral elements is not easily achievable and thus the accuracy of solutions for the three grids presented in section (4) will now be addressed.

Results for the three lobed mixer grids will be compared in detail in the near field of the mixer ($0 - 3\lambda$). Comparisons further downstream will be presented in the form of global quantities only. Figure 9 presents results obtained at four axial planes for the three different grids. Results are presented in terms of streamwise velocity contours normalised with the average velocity of the two streams (U_r). Also shown are the corresponding cross-sectional grids at each location. Figure 9(a) illustrates the formation and evolution of the shear layer downstream of the lobed mixer trailing edge for the purely hexahedral grid. Although the computations presented for the purely hexahedral grid in Fig. 9(a) were obtained on a grid consisting of only 150,000 nodes, the velocity contours are extremely similar to the results presented in Salman et al. [5] using a structured mesh consisting of approximately 700,000 nodes. The results for the present hexahedral grid will therefore be used as a reference set against which the contour plots of other predictions will be compared.

Results for the tetrahedral grid are presented in Fig. 9(b). Beginning at location $x/\lambda = 0.25$, the grid is clearly seen to be finely clustered along the mixer's trailing edge. Already at this location the velocity contours exhibit a noticeably different distribution within the shear layer from Fig. 9(a)(i). In particular, the low velocity contours ($U/U_r < 0.625$) have been smoothed out significantly. These contours are associated with the boundary layers on the mixer's surface. When present, additional high gradients within the shear layer exist. The higher level of smoothing in the tetrahedral grid has therefore contributed to the smoothing of these gradients. Another significant difference seen at this location is near the lobe trough of the low speed flow indicating a stronger rotation of the shear layer in comparison to the hexahedral results. Further downstream, the grid is gradually coarsened as seen in Figs. 9(b)(ii-iv) to allow a similar number of nodes to be used in all the cases studied. The resulting effect on the shear layer is higher numerical diffusion evident from the higher spreading of the shear layer. Additionally, due to the convoluted shape of the shear layer, it is not possible to distribute nodes efficiently. An increase in numerical smoothing is noticed as the shear layer moves into relatively coarse parts of the grid. An example of this is seen at location $x/\lambda = 1.0$ in Fig. 9(b)(ii) where a small part of the shear layer remains aligned with the vertical mixer walls. This portion is clearly less diffused than those that have migrated further out into the coarser regions of the grid, particularly if compared to the hexahedral solutions. An important feature to draw from location (ii) in Fig. 9(b) are the stronger kinks present in the shear layer when compared to corresponding results from the hexahedral grids. This implies the streamwise vorticity responsible for this rotation is stronger than in the hexahedral case despite the higher level of numerical smoothing present. This behaviour will be addressed later after studying other aspects of the results. Numerical smoothing continues further downstream to cause the shear layer to become highly smeared by $x/\lambda = 3.0$.

The results presented so far are indicative of the same numerical issues encountered in the study of the 2D planar shear layer. In that study, the mixed grid provided the best approach in terms of solution accuracy and computational cost. Results for the mixed grid of the lobed mixer are shown in Fig. 9(c). Generally, the results for this grid configuration are in much better agreement with the hexahedral results. While the shear layer remains in the hexahedral part of the grid (e.g. at $x/\lambda = 0.25$ and $x/\lambda = 1.0$), the shear layer structure is seen to be very similar to that in Fig. 9(a). The level of shear layer movement is essentially identical in both the hexahedral and mixed grids. Further downstream, the shear layer remains very well captured with higher numerical diffusion occurring only locally, mainly in the tetrahedral regions.

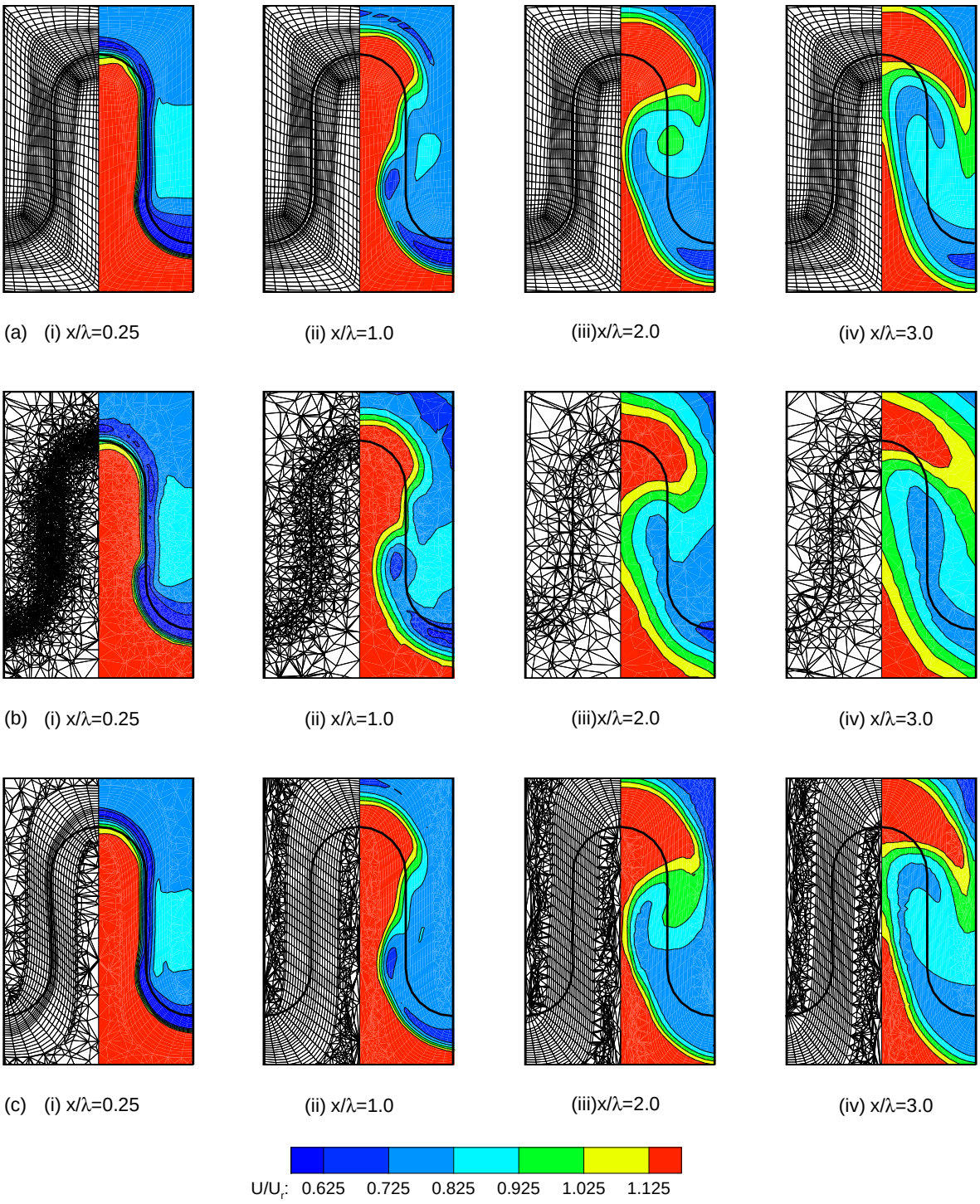

Figure 9: Normalised streamwise velocity contours with cross-sectional grids at corresponding locations; (a) Hexahedral grid, (b) Tetrahedral grid, (c) Mixed grid

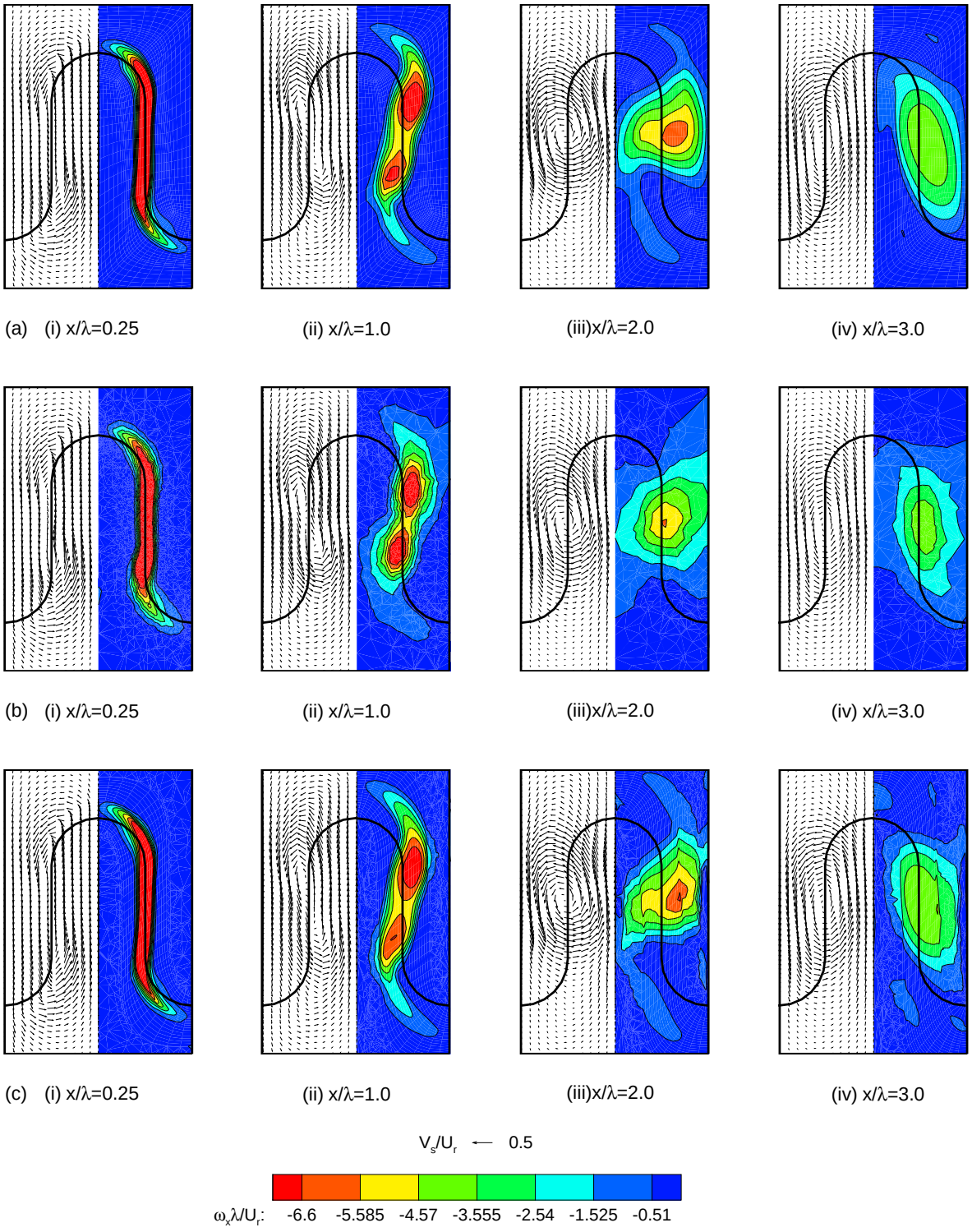

Figure 10: Normalised streamwise vorticity contours and corresponding secondary velocity vectors; (a) Hexahedral grid, (b) Tetrahedral grid, (c) Mixed grid

Due to the complex nature of the lobed mixer flow field, it is not sufficient to consider only the streamwise velocity field. Therefore, results of secondary velocity vectors and normalised streamwise vorticity contours are shown in Fig. 10. Again, results of the hexahedral case will be used as a reference set. Figure 10(a) shows a vorticity field concentrated along the mixer trailing edge following the interaction of the two streams. As the vorticity field evolves, two vortex structures become identifiable by $x/\lambda = 1.0$. These merge at $x/\lambda = 2.0$ and become more dissipated at $x/\lambda = 3.0$. The tetrahedral grid predictions show the same general behaviour. However, at $x/\lambda = 1.0$ the vorticity field indicates a stronger mutual interaction between the two vortices in comparison to the hexahedral case. This agrees with the strong kinks observed in the velocity contour plots. Further downstream, a single vortex structure exists with the vorticity contours revealing a much more distorted distribution. As in the velocity contours, solutions of the mixed grid show great similarity in the first two axial locations with the hexahedral results. Further downstream, despite the vorticity field being somewhat distorted, the levels and distributions still resemble results of the hexahedral case closely.

Focus so far has been on the near field. To quantify the level of mixing taking place throughout the entire mixing region, evaluations of the momentum thickness and streamwise circulation are carried out. The momentum thickness provides a measure of the momentum entrained into the shear layer and is evaluated from

$$\theta = \frac{2}{\lambda} \int_0^{\frac{\lambda}{2}} \int_{\frac{-3\lambda}{2}}^{\frac{3\lambda}{2}} \frac{(U - U_{low})(U_{high} - U)}{(U_{high} - U_{low})^2} dz dy \tag{5.2}$$

The inner integral in Eqn. (5.2) is evaluated over shear layer regions in the interval $-\frac{3\lambda}{2} \leq z \leq \frac{3\lambda}{2}$ where the streamwise component of velocity lies within the bounds $0.99U_{low} \leq U \leq 0.99U_{high}$. Figure 11(a) shows the variation of momentum thickness with downstream distance for the three grids studied. The results indicate a very similar growth of the mixing layer with downstream distance for the hexahedral and mixed grids. The tetrahedral grid shows a much more rapid growth of the mixed out region with a 50% error present as early as $x/\lambda = 1.0$. This supports the higher spreading observed earlier in the velocity contours with this grid. Further downstream, the mixing rate decreases substantially. The momentum thickness can be used to provide a measure of the effective mixing length required to allow complete mixing to be reached. Whereas this occurs by $x/\lambda = 5.0$ in the tetrahedral grid, a value of $x/\lambda > 10.0$ is implied by the other two cases. Such erroneous predictions with the tetrahedral grids can have severe implications if this design parameter is used to provide an estimate of the required mixing duct length for a gas turbine engine.

The streamwise vorticity field can be quantified by evaluating the streamwise circulation given by

$$\Gamma = \oint_C \mathbf{u} \cdot d\mathbf{s} \tag{5.3}$$

The contour integral used in Eqn. (5.3) is defined in Fig. 2. The contour dimensions used extended over the height of the computational domain. It is usual to normalise this value of the circulation with the value at the trailing edge obtained from the inviscid theory of Skebe [8] which states that

$$\Gamma = C_l U_r H tan(\varphi) \tag{5.4}$$

where $C_l = 4$ for mixers with parallel side walls, H is the lobe amplitude (half the lobe height, h), and φ is the lobe inclination angle. Results of the streamwise circulation for the

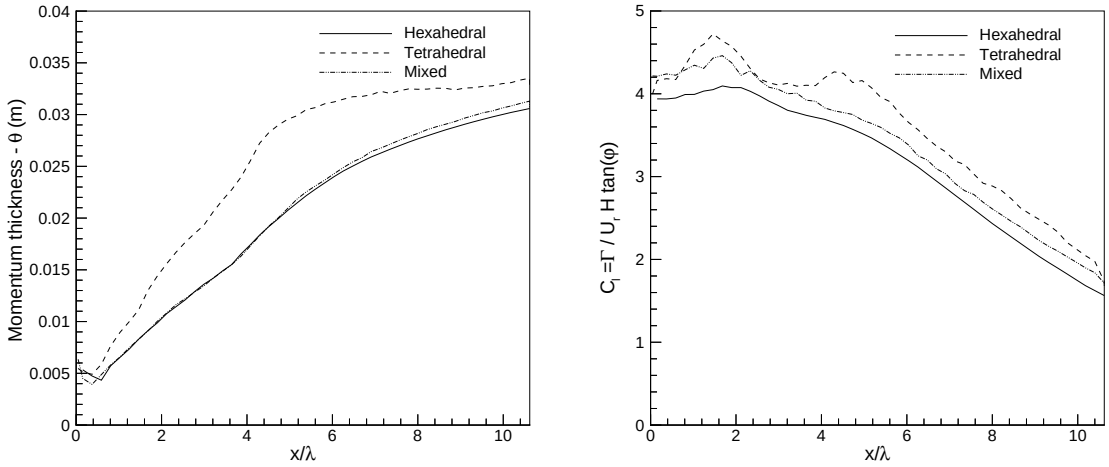

(a) Momentum thickness

(b) Normalised streamwise circulation

Figure 11: Variation of global quantities with downstream distance

three grids are shown in Fig. 11(b). A comparison of the results between the hexahedral and mixed grids reveals a higher value of the circulation at the trailing edge in the mixed grid. This is possibly due to slightly better resolution of the lobe surface boundary layer due to the finer axial clustering of the mixed grid. Within the mixing region, similar trends exist in the two cases with the initial higher value of the circulation in the mixed grid persisting downstream. The circulation for the tetrahedral grid is characterised by peaks occurring at $x/\lambda = 1.5$ and $x/\lambda = 4.5$. Otherwise, similar trends to the other cases are observed further downstream despite the higher level of circulation. Referring back to the vorticity plots, of particular interest was the higher level of vorticity which existed at $x/\lambda = 1.0$. The first peak in the streamwise circulation clearly reflects this. To understand this higher circulation level predicted with the tetrahedral grid, a look at the predicted turbulent field is needed. The location $x/\lambda = 1.0$ has been identified as a region of interest. The turbulent kinetic energy at this location for the three cases is therefore shown in Fig. 12. This has been normalised with the square of the average velocity of the two streams. The turbulent energy shows regions of high turbulence within the shear layer. Peak values are found concentrated at the locations where the two vortices are located. Comparing the three cases, the hexahedral and mixed grids show a very similar distribution and peak values. The main differences are seen in the spiralling 'arms' of the shear layer where the mixed grid shows a less spread out distribution. In stark contrast, the tetrahedral grids show much lower peak values of the turbulent energy. The low turbulence levels that do exist are also more highly diffused than the other cases.

Turbulence is generated in regions of high gradients. Numerical smoothing destroys these gradients. As the gradients are smoothed out, the mechanism through which turbulence and hence eddy viscosity is generated is removed. Due to the nonlinear form of the production terms in the $k - \epsilon$ model a significant reduction results. This same mechanism was also observed in the planar shear layer. While numerical mixing has increased in the tetrahedral grid, the turbulent mixing has been significantly under predicted. This strong coupling between the turbulent field and the mean flow can result in regions where the total mixing has reduced locally. This mechanism could have attributed to the higher levels of vorticity observed at

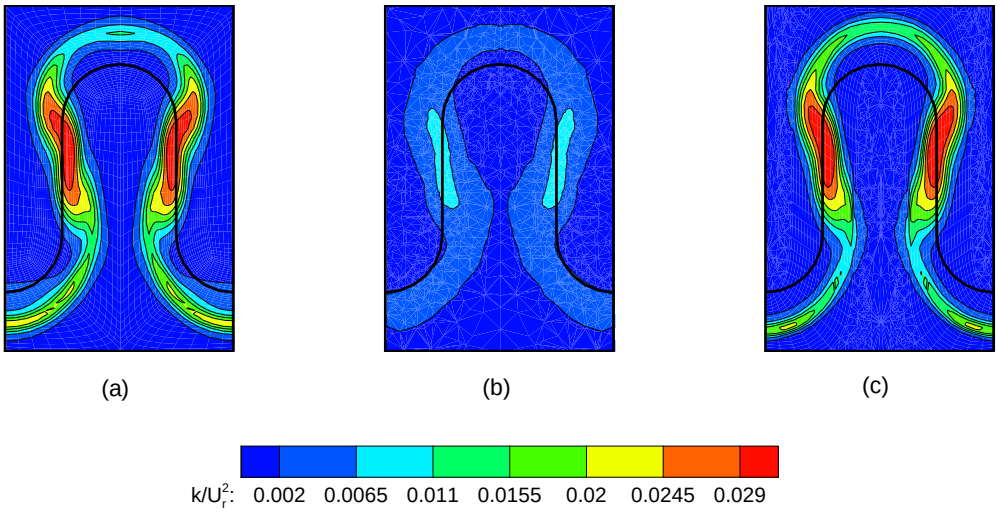

Figure 12: Normalised turbulent kinetic energy contours at $x/\lambda = 1.0$; (a) Hexahedral grid; (b) Tetrahedral grid; (c) Mixed grid

$x/\lambda = 1.0$ in the tetrahedral grid. While most of the shear layer has spread through numerical diffusion, regions where the two vortices exist clearly contain much lower turbulent mixing. The combined effect is then lower dissipation of the vorticity field as suggested by the higher levels of streamwise circulation.

The evidence presented above indicates that tetrahedral grids are not well suited for such mixing applications. In contrast, hexahedral and mixed grids provide much better predictions. The full potential of unstructured methods can only be realised when including adaptive techniques. The study conducted here has indicated that a hybrid adaptive method may provide the highest quality solutions at the lowest computational costs.

6 CONCLUSIONS

Results have been presented for the evolution of a planar and convoluted turbulent shear layer showing the influence of grid type on the accuracy of the prediction. When comparing different grid types, similar numbers of nodes were used.

Shear layer flows have the characteristic of a predominant flow direction with strong gradients normal to that direction. Hexahedral grids were found to be well suited to this type of flow, the alignment of faces with these two directions gave acceptable levels of numerical smoothing and so correct prediction of the turbulent shear layer growth for a given number of node points. However, a tetrahedral grid with a similar number of nodes gave spurious excess mixing due to numerical smoothing in the initial mixing region, followed by a reduction in mixing rate further downstream due to under prediction of turbulence kinetic energy. These results were confirmed for the convoluted mixing layer. The anomalous results from the tetrahedral grid arise because of the presence of control volume faces that are not aligned with either of the streamwise or cross stream directions - the presence of both a gradient and a flow direction across the face triggers numerical smoothing that is larger than the physical diffusion. Increasing the aspect ratio of triangular elements reduces the numerical smoothing and improves the prediction of the shear layer spreading rate.

In the convoluted turbulent shear layer, the spurious numerical diffusion due to the tetrahedral grid gives an increased peak vorticity immediately downstream of the mixer. More rapid mixing ensues and analysis of momentum thickness indicates that complete mixing occurs by five lobe wavelengths downstream, whereas the hexahedral and mixed hexahedral/tetrahedral/pyramidal grid agree with a fine grid hexahedral solution of complete mixing by a distance greater than ten lobe wavelengths. In a design scenario, the required mixing duct length found from a tetrahedral grid solution may be too short.

A mixed grid with aligned high aspect ratio hexahedral elements in the shear layer region and pyramids and tetrahedra linking to the outer domain appears to be the optimal grid for this type of problem. However, grid alignment for the convoluted shear layer would require the use of an adaptive method.

ACKNOWLEDGEMENTS

The authors would like to acknowledge funding support for the research work reported here from the Engineering and Physical Sciences Research Council (UK), Grant No. GR/L17863. Financial assistance and technical review monitoring was also provided by Rolls-Royce and DERA; the authors would like to thank in particular Dr. Leigh Lapworth (RR), Dr. Jens-Dominik Müller (Oxford University) and Prof. Michael Giles (Oxford University).

References

[1] S.R. Allmaras, 1993. Analysis of a local matrix preconditioner for the 2-D Navier-Stokes equations. *AIAA 93-3330-CP.*

[2] B.E. Launder and D.B. Spalding, 1974. The numerical computation of turbulent flows. *Computer Methods in Applied Mechanics and Engineering*, **3**: 269–289.

[3] W. Konrad M. Lötzerich and P.J.R. Strange, 1994. Numerical and experimental parameter studies of lobed mixers. Technical Report 94-H2-127, Deutsche Gesellschaft für Luft und Raumfahrt.

[4] L. Martinelli, 1987. *Calculations of Viscous Flows with a multigrid method.* PhD thesis, Dept. of Mech. and Aerospace Eng., Princeton University.

[5] H. Salman J.J. McGuirk and G.J. Page, 1999. A numerical study of vortex interactions in lobed mixer flow fields. *AIAA Paper 99-3409.*

[6] P. Moinier, 1999. *Algorithm Developments for an Unstructured Viscous Flow Solver.* PhD thesis, Oxford University.

[7] R.W. Paterson, 1982. Turbofan forced mixer-nozzle internal flow field, part 1 - A benchmark experimental study. Technical report, NASA CR 3492.

[8] S.A. Skebe R.W. Paterson and T.J. Barber, 1988. Experimental investigation of three-dimensional forced mixer lobe flow fields. *AIAA Paper 88-3785-CP.*

[9] N.A. Pierce, 1997. *Preconditioned Multigrid Methods for Compressible Flow Calulations on Stretched Meshes.* PhD thesis, Oxford University.

[10] P.L. Roe, 1981. Approximate Riemann solvers, parameter vectors, and difference schemes. *Journal of Computational Physics*, **43**: 357–372.

[11] E. Morano M.H. Lallemand M.P. Leclercq H. Steve B. Stoufflet and A. Dervieux, Berlin 1991. Local iterative upwind methods for steady compressible flows. *In* Springer-Verlag, editor, *Third European Conference on Multigrid Methods*, page 227.

[12] M.N. O'Sullivan J.K. Krasnodebski I.A. Waitz E.M. Greitzer C.S. Tan and W.N. Dawes, 1996. Computational study of viscous effects on lobed mixer flow features and performance. *Journal of Propulsion and Power*, **12**(3): 449–456.

[13] D.C. Wilcox, 1994. *Turbulence Modeling for CFD.* DCW Industries, Inc.